REPTILE SLEEP

Slow waves, sharp waves, ripples, and REM in sleeping dragons

Mark Shein-Idelson,* Janie M. Ondracek,* Hua-Peng Liaw,† Sam Reiter,† Gilles Laurent‡

Sleep has been described in animals ranging from worms to humans. Yet the electrophysiological characteristics of brain sleep, such as slow-wave (SW) and rapid eye movement (REM) activities, are thought to be restricted to mammals and birds. Recording from the brain of a lizard, the Australian dragon *Pogona vitticeps*, we identified SW and REM sleep patterns, thus pushing back the probable evolution of these dynamics at least to the emergence of amniotes. The SW and REM sleep patterns that we observed in lizards oscillated continuously for 6 to 10 hours with a period of ~80 seconds. The networks controlling SW-REM antagonism in amniotes may thus originate from a common, ancient oscillator circuit. Lizard SW dynamics closely resemble those observed in rodent hippocampal CA1, yet they originate from a brain area, the dorsal ventricular ridge, that has no obvious hodological similarity with the mammalian hippocampus.

It is now generally agreed that animals ranging from invertebrates to humans sleep. The principal attributes of sleep are shared by all animals and define what is often described as "behavioral sleep," which has been identified in many invertebrates and vertebrates (*1*–*8*). The first electrophysiological studies of sleep were conducted in humans and revealed clear electroencephalographic (EEG) correlates of brain states during sleep (*9*–*11*). Researchers now divide mammalian sleep EEG patterns into two main types: (i) slow-wave sleep (SWS) and (ii) non-SWS or REM sleep (REMS), which is accompanied by conspicuous rapid eye movement (REM) and an otherwise atone axial and limb musculature (*12*). So far, these electrophysiological attributes of sleep have been demonstrated only in mammals and birds (*7*, *13*–*17*).

Mammals and birds belong to different branches of an early bifurcation of the amniotes, which occurred over 300 million years ago (Fig. 1A). Because mammals and birds are the only homeotherms among living vertebrates, and because it has been thought that only they manifest REMS and SWS, it has been suggested that REMS and SWS are the expression of convergent evolution driven by common constraints and selective pressures correlated with homeothermia (*18*, *19*). REMS and SWS, however, could be ancestral to mammals and birds; if so, their electrical signatures should also exist in nonavian reptiles. Evidence for such signatures from sleeping reptiles has thus far been inconclusive (*1*, *14*, *15*, *17*, *18*, *20*–*22*). We reexamined this issue by recording from the brain of a lizard, the Australian dragon *Pogona vitticeps*. Because lizards belong to the lepidosaurs, the earliest subclass to branch out from the sauropsid trunk and thus the one that is most distant from avians (*23*), *Pogona* is ideal for examining the evolution of sleep among amniotes.

We confirmed the existence of behavioral sleep in adult *Pogona* dragons (Fig. 1, B and C, and fig. S1) (*24*). Behavioral sleep features were highly consistent across individual lizards and nights (Fig. 1C), and the transition between awake and behavioral-sleep states usually anticipated the programmed transition from light to dark. We implanted five lizards with either tetrode arrays (*25*) or linear silicon probes inserted in the dorsal forebrain (in the cortex and the dorsal ventricular ridge, or DVR). After recovery from surgery and slow electrode advance, we recorded extracellular electrical activity [local field potential (LFP), multi- and single-unit activity] continuously over 18 to 20 hours centered on the middle of the night, usually combining behavioral monitoring with electrophysiology. Recordings from individual animals were repeated over days to weeks.

LFP recordings from the DVR in the middle of the animals' behavioral sleep revealed a slow oscillation (red, Fig. 2A) and negative deflections of varying amplitude. Nocturnal LFPs could be segmented into two principal spectral clusters (Fig. 2B): (i) segments of low-frequency activity (<4 Hz, δ band; Fig. 2Ac; blue in Fig. 2C and fig. S2A) and (ii) segments of broadband activity (Fig. 2Ad; red in Fig. 2C), which were more similar to activity in the awake state (fig. S2, B to D). The frequency at which the curves of these two components intersected ($F_{trans.}$; Fig. 2C) was around 4 Hz and stable across animals and nights (Fig. 2D). We observed neither 10 to 15–Hz spindles nor clear activity in the 5 to 10–Hz (θ) band. By analogy with metrics that have been used with rodents (but to account for the absence of dominant θ-band activity in sleep), we chose the 10 to 30–Hz (β) band to quantify the broadband activity cluster and computed the ratio of δ to β power (rather than δ to θ power, as with rats) (*26*, *27*) over a sliding window. For a duration of 6 to 10 hours, starting shortly after the onset of imposed darkness and ending 1 to a few hours before the lights were turned on, the δ/β ratio oscillated regularly and continuously (Fig. 2E and figs. S3 and S4) with a period of about 80 s (Fig. 2F and fig. S4). We call this epoch "electrophysiological sleep" (e-sleep). E-sleep started shortly after the onset of behavioral sleep and ended 0.5 to several hours before the end of behavioral sleep (Fig. 2E). In all cases, e-sleep represented a dominant and continuous fraction of behavioral sleep (Fig. 2E and fig. S4).

The period of the δ/β oscillation was temperature-dependent. After initial recordings in animal 1 (temperature, ~25°C; period, >100 s; Fig. 2G), we raised and stabilized room temperature to 27°C. The mean oscillation period decreased to around 80 s. In one further experiment, we raised the temperature to 32°C, and the oscillation period further decreased to ~60 s [asterisk (animal 5), Fig. 2G]. Over a single night at constant temperature, the oscillation period typically increased slowly (by ~2 s/hour on average) from evening to morning (figs. S4 and S5). The envelope amplitude of the δ/β oscillation varied to a much greater extent, typically ramping up at the beginning and down at the end of the night, but with wide instantaneous variations (fig. S4). Similar results were obtained by analyzing the δ and β bands separately (rather than their ratio) (fig. S6).

δ power during SWS primarily reflected the repeated occurrence of large negative deflections of LFP (halfwidth, 100 to 400 ms at 27°C) at a rate of less than one per second (Fig. 2, A to Ac). Because their shape was relatively stereotyped, an averaged template could be obtained (Fig. 2Ae, red) and used to detect most events automatically from a night's recording. High-pass (HP) filtering of these selected LFP segments revealed that they nearly always contained short bursts of >70-Hz multi-unit activity, which were locked to the deflection's descending phase (Fig. 2Ae, bottom trace). The reliability of this association of HP and LFP features is illustrated by 1000 consecutive events (Fig. 2Af). By analogy with classical observations in rodent hippocampal CA1 (*26*–*30*), we will call the LFP events "sharp waves" and the corresponding HP events "ripples." They are each slower than their rat counterparts, possibly as a result of temperature differences (27°C in this study versus the 37° to 38°C body temperature of rats). The reliability of this sharp wave–ripple (SWR) association is illustrated in Fig. 2H (five animals, 18 nights).

In mammals, non-SWS is usually accompanied by eye movements (*10*–*12*, *31*). We thus tested whether this is the case in sleeping lizards. We monitored the eye contralateral to the LFP-recording site with infrared cameras and quantified eye movement by computerized video analysis (Fig. 3A, movie S1, and materials and methods). The eyes twitched during the night in discrete epochs interposed with immobility or slow drift. When matched against a simultaneously recorded contralateral LFP, REM occurred preferentially when δ/β was low—i.e., in

Max Planck Institute for Brain Research, Frankfurt am Main, Germany.
*These authors contributed equally to this work. †These authors contributed equally to this work. ‡Corresponding author. Email: gilles.laurent@brain.mpg.de

alternation with SWS (Fig. 3B and movie S1). Because δ/β was periodic, we measured the phase of eye movements relative to that of δ/β (red dots in Fig. 3, B and C). These measurements confirmed that REMS alternates with SWS and showed that eye movements occur preferentially in the quarter cycle before δ/β power reaches its minimum (Fig. 3, C to E). Hence, the lizard's two e-sleep states (high and low δ/β) fit phenotypically those classically described in mammals (SWS and REMS, respectively). These two states alternate in a clock-like fashion, defining up to 350 consecutive cycles per night, with SWS occupying just under 50% of each cycle on average (fig. S7). We next examined spiking activity during the two sleep states.

Instantaneous DVR firing frequencies during sharp waves were high (~100 Hz; Fig. 4A). These peaks, however, arose on top of an average SWS firing rate that was close to zero (Fig. 4A). In contrast, spiking activity during REMS was high, reaching values similar to those recorded in the awake state (stippled lines in Fig. 4B). The DVR ripples are thus short high-frequency bursts that correspond to sharp waves during SWS, intermittently interrupting a "silent" background (e.g., black trace at the top of Fig. 4A). Mean firing rates, however, slowly oscillate over the sleep cycle between near silence (SWS) and awake-like rates (REMS).

Given the apparent similarity between these SWRs and those described in rat hippocampal CA1 (*26*–*29*), we had initially expected our recordings to be centered in the lizard's putative hippocampal regions (cortex). Using micro-computed tomography (μ-CT) scans (fig. S8) and small electrolytic lesions followed by histology, we found unexpectedly that all SWS and REMS activity described above originated from the anterior DVR (Fig. 4C and fig. S9) and not from the cortex. Activities in the anterior DVR and cortex were correlated, however (fig. S10A). Immediately before the onset of a sharp wave (trough at time t = 0; Fig. 4D), firing probability decreased in cortical and DVR neurons. The spikes in Fig. 4, D and F, originated from 5000 sharp waves recorded during one night; single-neuron firing probabilities during SWS are thus extremely low, especially in the DVR, which is consistent with population data. Hence, phasic inhibition could be detected in single cells only if activity was examined over many individual sharp waves (Fig. 4, D and F), or when derived from population averages (Fig. 4G). About 100 ms before the trough of the sharp wave and coincident with its rapid onset (Fig. 4, D and G), DVR neuron activity increased sharply, and individual neurons fired only a few action potentials, if any (Fig. 4D), as observed in rat CA1 (*26*, *32*, *33*). As the sharp wave ended, the probability of DVR neuron firing declined sharply back to zero (Fig. 4, F and G).

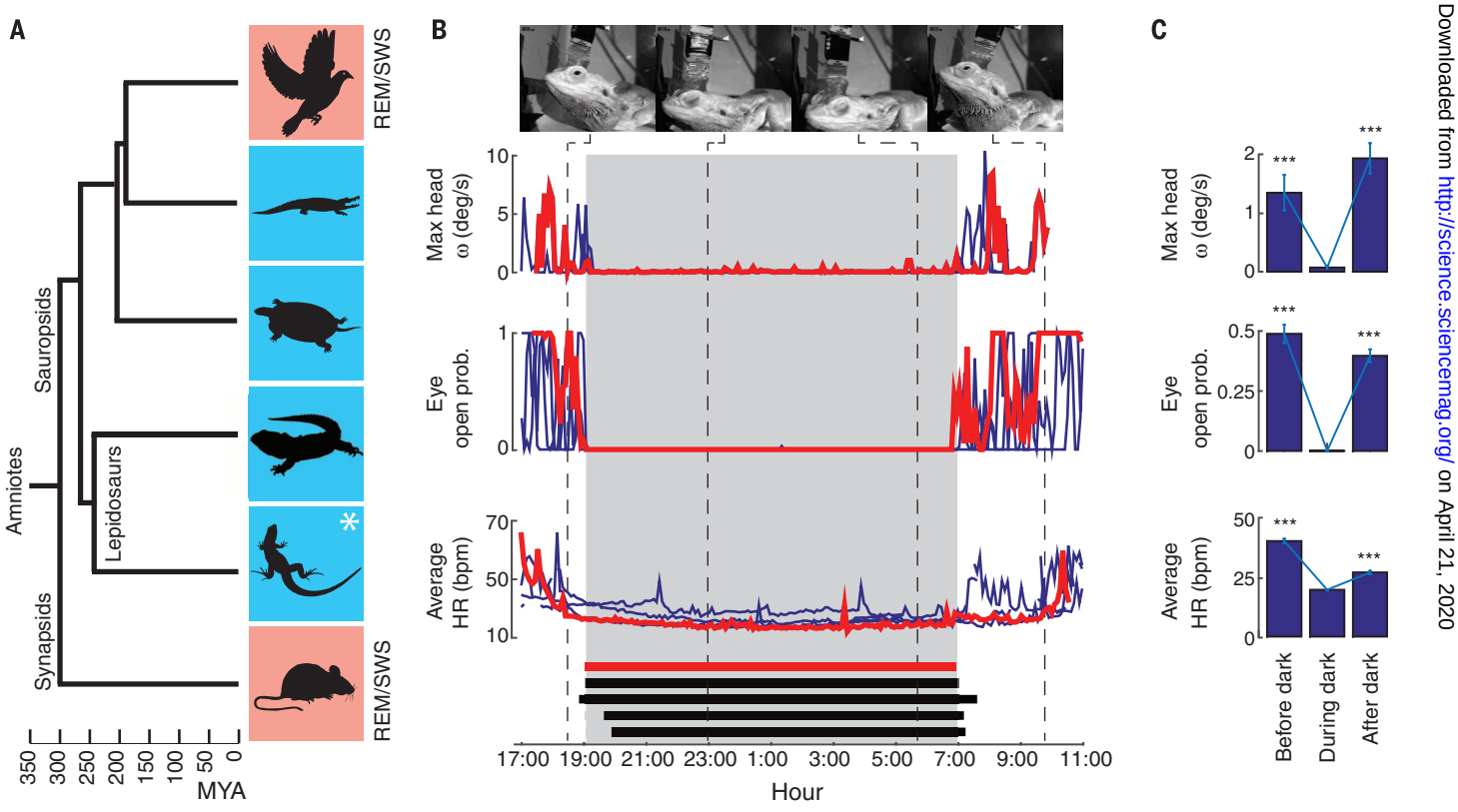

Fig. 1. Behavioral sleep in a reptile, the Australian dragon *Pogona vitticeps*. (**A**) Cladogram of vertebrate evolution, indicating those classes (avians and mammals; pink boxes) in which the electrophysiological signatures of vertebrate sleep (SWS and REMS) have been established. These classes are also characterized by homeothermia. Blue boxes denote the nonavian reptiles [from top to bottom: crocodilians; chelonians; tuatara (*Sphenodon*); and squamates (marked with an asterisk), including lizards and snakes], all of which are poikilotherms. *Pogona* is an agamid lizard. MYA, million years ago. The time scale follows (*23*). (**B**) Behavioral and physiological parameters used to assess the behavioral-sleep state in *Pogona* (red traces are from the animal pictured; blue traces are from other nights and animals). The top row includes representative photographs illustrating the awake (far left and far right) and sleep (middle) states. The second row shows maximum head angular velocity (ω, degrees per second) during and around nighttime (n = 3 recordings). Stationarity tends to precede the onset of darkness (gray shaded area). Plotted are peak values in successive 5-min periods. The third row shows the probability of the eye contralateral to LFP recording being open (n = 4 recordings). This probability was calculated over all movie images in successive 5-min segments. The fourth row shows heart rate (HR) in beats per minute, plotted as successive 5-min averages (n = 5 recordings from three animals). Curve interruptions (in awake segments) are due to animal movements, preventing reliable HR measurement. The bars in the fifth row indicate the periods defined as behavioral sleep, determined as the intersection of rest periods, as assessed from the above physiological and behavioral parameters (see the materials and methods section in the supplementary materials) (n = 5 recordings from three animals). Behavioral sleep is tightly aligned with the light-dark cycle, but the transition to behavioral sleep often anticipates the onset of darkness, as evident in head angular velocity, eye-open probability, and HR measurements (fig. S1 shows data from unoperated animal). (**C**) Means and SEM of the variables in (B), calculated over successive 5-min segments before, during, and after dark. ***P < 0.001; two-tailed t test with Bonferroni correction.

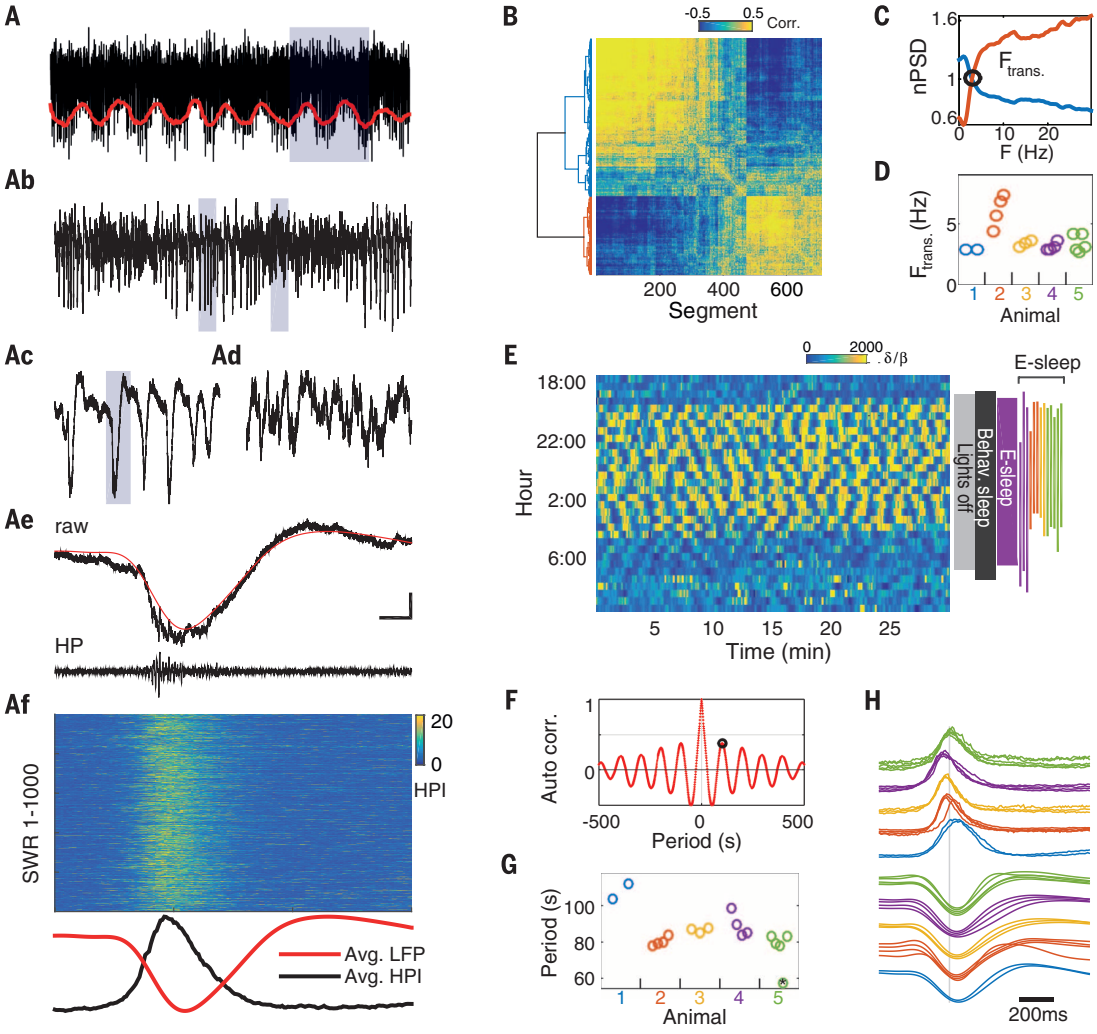

Fig. 2. Behavioral sleep includes a long uninterrupted epoch of regularly alternating SWS and non-SWS, defining e-sleep. Salient features of unfiltered LFP recorded in the DVR during sleep are shown in A to Af; all of these data are from the same animal and night. (**A**) Slow time base. The LFP envelope oscillates slowly, as evident in the order-filtered trace (red). The shaded area is expanded in (Ab). (**Ab**) Two alternating epochs are apparent, with and without large negative LFP spikes, with intermediate-sized deflections in between. The shaded areas are expanded in (Ac) and (Ad). (**Ac**) Stereotypical negative LFP spikes with positive rebound occur regularly every 1 to 3 s. The shaded area is expanded in (Ae). (**Ad**) The epoch alternating with that in (Ac) lacks stereotypical LFP spikes. (**Ae**) Close-up view of the shaded LFP spike in (Ac) (top, black) and the averaged template (red, average of 1000 LFP spikes aligned on the troughs). The same single trace is shown below after high-pass filtering (60 to 900 Hz). This combination resembles the mammalian SWR complex. (**Af**) One thousand successive ripples (HPI, HP signal intensity) aligned, for each trace, on the peak cross-correlation between the corresponding LFP waveform and the template [red trace in (Ae)]. Averages of all 1000 matching HPI (black) and LFP (red) traces are shown below. The horizontal scale bar is 90 s for (A), 20 s for (Ab), 2 s for (Ac) and (Ad), and 139 ms for (Ae). The vertical scale bar is 300 μV for (A) and (Ab), 200 μV for (Ac) and (Ad), and 180 μV for (Ae). (**B**) Night LFPs define two main spectral clusters. Shown is an ordered correlation matrix of spectral characteristics, calculated from 10-s data segments from one LFP channel over one night. Two dominant clusters are evident. The dendrogram (left) is based on a Euclidian metric that uses Ward linkage. The original data are the same as in (A) to (Af). (**C**) Normalized power spectral density (nPSD) of the nighttime LFP for the two clusters in (B). $F_{trans.}$ is the frequency at which curves intersect (~4 Hz). One cluster dominates with higher-than-average power at low frequencies (δ), defining SWS and corresponding to LFP segments containing SWRs [as in (Ac)]. The other cluster (β) dominates with higher power at $F > F_{trans.}$ (see also fig. S2). (**D**) $F_{trans.}$ measured across animals and nights (each circle is a night). The variance is low (except for animal 2, in which the signal-to-noise ratio was lowest). (**E**) Epochs of high and low δ power oscillate regularly throughout the night, forming a continuous period of e-sleep. The evolution of the δ/β power ratio (measured piecewise over 10-s moving windows shifted in 1-s steps) around nighttime is plotted on the left for one animal. Each horizontal row represents a 30-min segment (running left to right); successive 30-min segments run continuously from top to bottom. This slow alternation (high versus low δ) starts shortly after the lights are turned off and continues uninterrupted until less than an hour before the end of behavioral sleep (though with smaller-amplitude modulation in the last 2 hours). Epochs of behavioral sleep and e-sleep (defined by δ-power alternation) for this animal are shown on the right. The thin vertical bars are epochs of e-sleep for this (purple) and three other animals over several nights each, showing the consistency of the pattern. E-sleep occupies a major fraction of behavioral sleep and usually occurs toward the beginning of it (figs. S3 and S4). (**F**) Autocorrelation function of the e-sleep δ/β data in (E). The average period (circled) is around 80 s (27°C) (see also fig. S5). (**G**) Period of the autocorrelation function [measured as in (F)] across five animals and 18 nights, showing relative consistency for each animal. Both nights for animal 1 were at 25°C. All nights for animals 2 to 4 were at 27°C. Animal 5 spent four nights at 27°C and one night (*) at 32°C. (**H**) Averaged SWR components (top five sets, HPI; bottom five sets, LFP) for the animals in (G). The alignment is as in (Af).

Activity in the cortex also changed around individual sharp waves. Cortical neuron firing rates decreased shortly before a sharp wave and then increased, less abruptly than in DVR neurons, to peak some 400 ms after the DVR population (Fig. 4, D, F, and G). This relationship between DVR and cortical firing during a sharp wave was observed in all cortical and DVR units along a recording probe (Fig. 4F) and aligned precisely with a correlation analysis of signal amplitude as a function of recording depth (Fig. 4E): Units with cortical activity were physically clustered and separated from the DVR-unit cluster by a region that lacked a high-frequency signal (the ventricle) (Fig. 4, E and F). These results were consistent across animals in single- and multi-unit data (Fig. 4, D, F, and G).

Last, we compared the modulation of firing rates of cortical and DVR neurons over sleep cycles. Both populations oscillated with the ~80-s period (fig. S10A) and were phase-locked with one another (Fig. 4H). Hence, SWR-related firing activities in the DVR and cortex occur near the nadir of their respective sleep-cycle modulation, and mean firing rates are always higher in the cortex than in the DVR (fig. S10, A to C).

Sleep-related brain dynamics similar to mammalian SWS (including SWRs) and REMS exist in *Pogona*, a nonavian reptile. This decreases the probability that SWS and REMS result from convergent evolution among homeotherms. Rather, it suggests that the circuits underlying the electrophysiological signatures of sleep evolved in a common ancestor early in amniote evolution, before the synapsid-sauropsid bifurcation over 300 million years ago, if not earlier (Fig. 1A). Sleep-related brain states should probably be reexamined in amphibians and fish as well.

Although similar to mammalian sleep, lizard SWS and REMS resemble a stripped-down (two-state) version of the richer mammalian repertoire (especially in comparison to sleep in large mammals). In *Pogona*, SWS and REMS alternate regularly throughout the night with a short period (~80 s), generating up to 350 SWS-REMS cycles (compared with four to five 90-min cycles in humans, in which the fraction constituted by REMS changes throughout the night) (*19*, *31*). Given the ancient origin of the brain areas associated with sleep in mammals (the thalamus, hypothalamus, and brainstem) (*34*–*39*), reptilian brain sleep may point to an ancestral control system for sleep-related brain dynamics. Reptiles could thus provide a useful experimental testbed for mechanistic models of SWS-REMS alternation.

The SWRs in lizards resemble those identified in rodent hippocampal CA1 (*26*, *28*). That they arise in the DVR is unexpected, because the region of the reptilian brain that is assumed to be equivalent to the mammalian hippocampus is the medial cortex, not the DVR (*23*, *40*). The cortex was inhibited just before the occurrence of DVR ripples and was excited immediately during and after them, in a pattern reminiscent of the correlation between hippocampal ripples and cortical spindles in rats (*26*). Does this then suggest hippocampus-like functions for the DVR? So far, no functional, hodological, or architectonic arguments exist to support this possibility. Oscillatory rhythms associated with SWS are not an exclusive property of the mammalian hippocampus; they are seen also in the neocortex

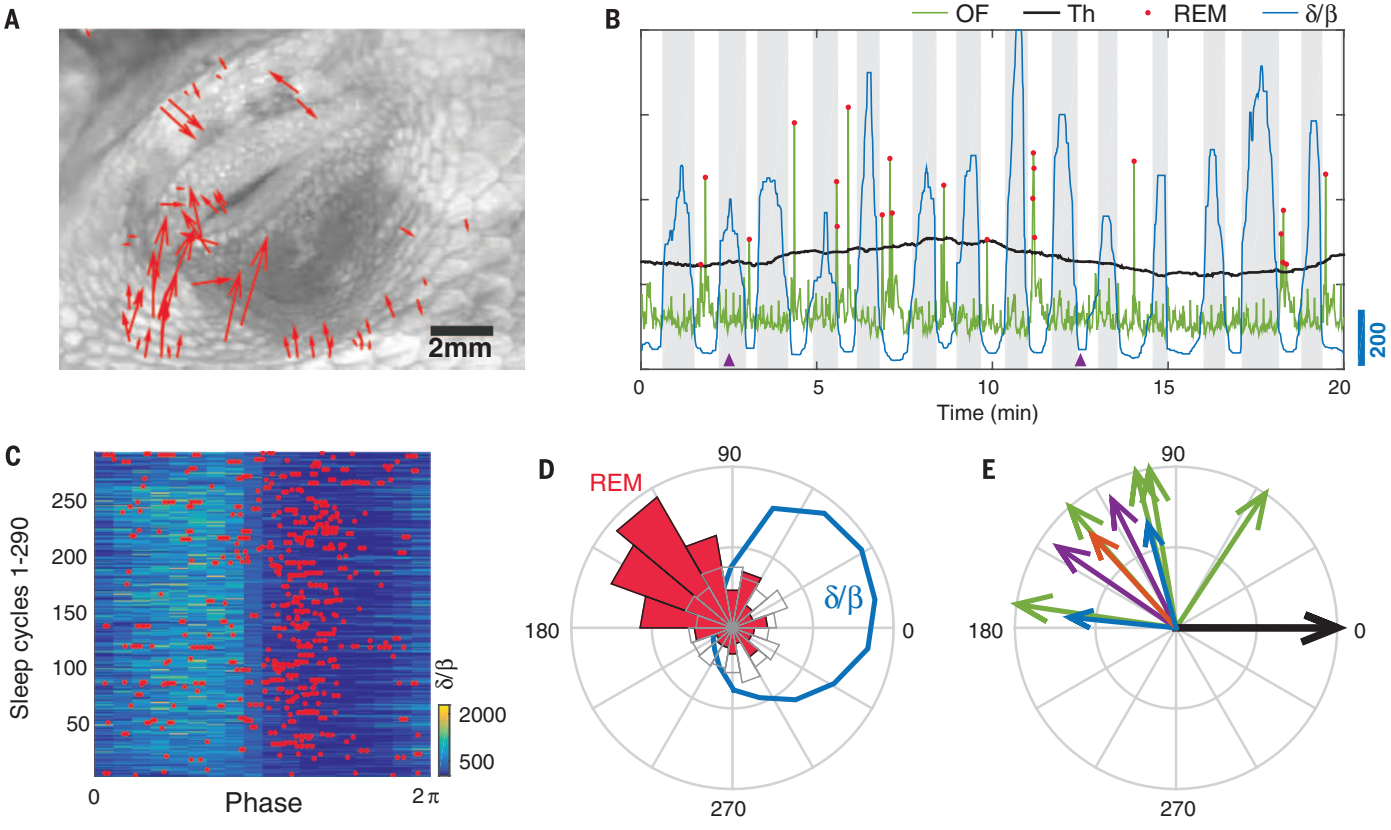

Fig. 3. Rapid eye movements alternate with SWS. (**A**) Quantitative analysis of videos of closed eyes reveals regular epochs of REM, detected as local flow fields of eyelid and orbital skin features (arrows) (movie S1). (**B**) The summed magnitude of these optical flow-field vectors (OF, green), plotted here as a function of time, peaks periodically and nearly always in periods of low δ/β LFP power (white bands). Using a floating threshold crossing (Th, black) for the detection of the fastest-motion events, the timing of peak eye movements was recorded (red dots). The epoch between the two purple arrowheads is shown in movie S1. (**C**) Because δ/β power is a near-periodic function of time during e-sleep (period, ~80 s), cycles can be normalized linearly, and the timing of eye movements [red dots, as in (B)] can be plotted relative to the phase of the cycle for a full night. Most eye movements cluster in the same phase (first half of the low-δ phase; dark blue). (**D**) Rose diagram of phases of eye movement (red) and SWS (high δ/β, blue) from the data in (C), confirming the phase shift between REMS and SWS. Shuffle control of the REM phase bias is shown in gray. (**E**) Polar plot of the mean phase angle of REMS relative to SWS (set at 0) for four animals (colors are as in Fig. 2) and 10 nights. The phase shift is consistent: 9 of 10 vectors are contained in the quarter cycle corresponding to the beginning of non-SWS. (Vector norms in the diagram are meaningless, except in indicating individual animals.)

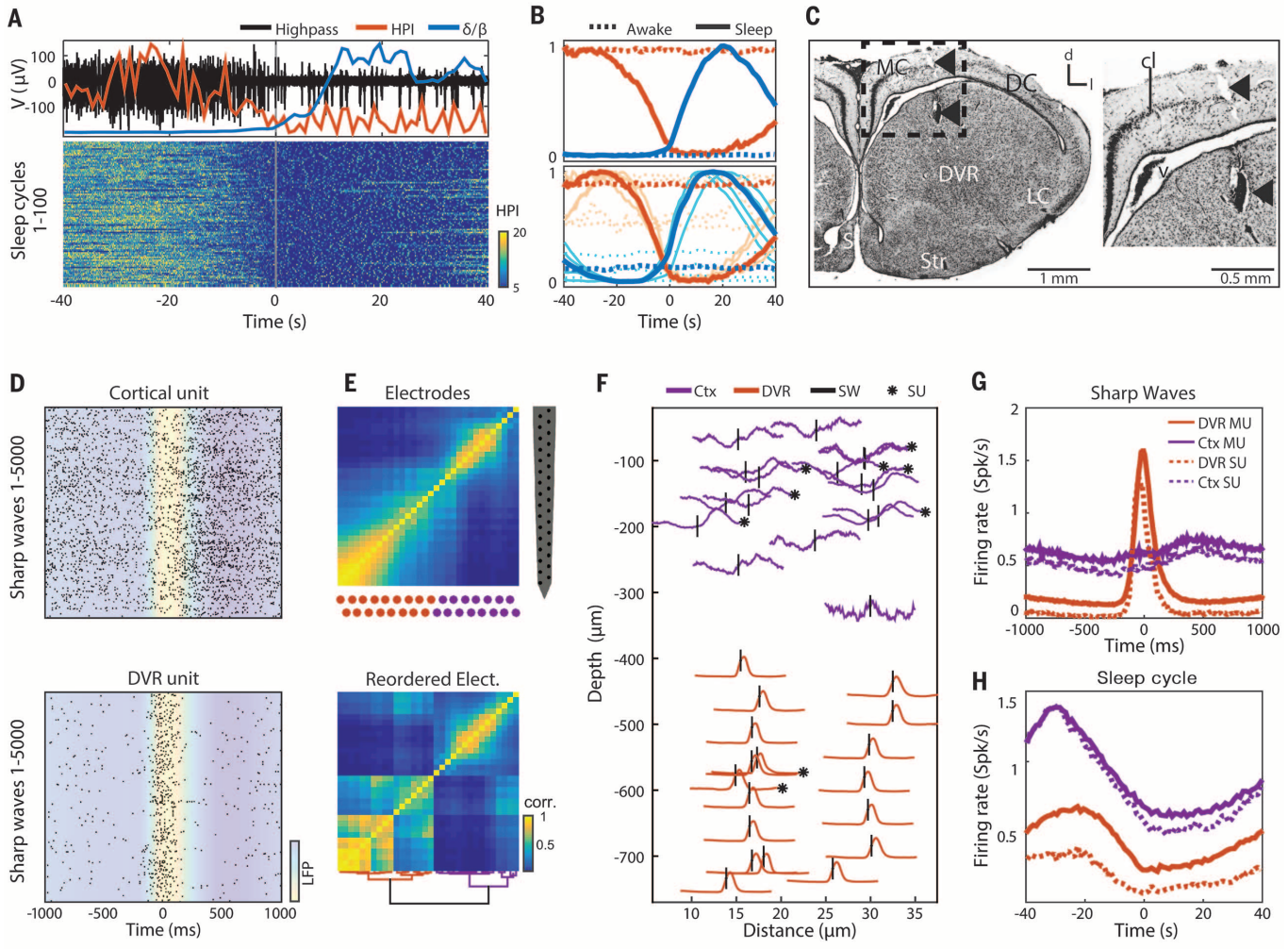

Fig. 4. Firing rates vary in antiphase with δ activity, SWRs originate in the DVR area, and DVR activity during sharp waves is correlated with activity in the cortex. (**A**) Firing activity (band pass, 0.1 to 2 kHz; black, top panel) is anticorrelated with δ/β (blue, top panel) around the sleep cycle (*V*, voltage). HPI (50-ms bins; materials and methods) was measured for each sleep cycle (red, top panel) and plotted for 100 successive sleep cycles (bottom panel). High-frequency bursts occur during the high-δ/β phase, as seen in the single trace (black) in the top panel, corresponding to individual sharp waves. (**B**) The relationship between firing and δ/β(*t*) is consistent and systematic across animals. The top panel shows means over all sleep cycles for a single animal [same lizard as in (A)]. Stippled lines (red, firing rates; blue, δ/β) indicate values measured during the awake state over consecutive 80-s segments. Peak firing rates during REMS (non-SWS) match those in the awake state. Maximum and minimum values measured during sleep (continuous lines) are normalized to range from 0 to 1, and values in the awake state are plotted in same normalized range. The bottom panel shows data from this and three other animals for all nights. The stippled curves (average values in the awake state) differ, due to variations across animals in the fraction of rest within the awake state. (**C**) Coronal section through a lizard's forebrain, showing the electrode track (along the two arrowheads) and main anatomical features. The area framed at left is magnified in the right panel (cl, cell layer; d, dorsal; l, lateral; DC, dorsal cortex; LC, lateral cortex; MC, medial cortex; S, septum; Str, striatum; v, ventricle) (figs. S8 and S9). (**D**) Simultaneous recording from one isolated cortical unit (top) and one DVR unit (bottom) around 5000 successive sharp waves. The alignment is on the trough of the sharp-wave LFP (color-coded) at $t = 0$. Each dot represents an action potential. (**E**) Physical clustering of HP intensities along the length of a multisite recording electrode (top right). Shown on the top left is a correlation matrix, ordered by physical position along the recording probe, of the HP intensities measured from each one of the 32 sites during REMS. Two principal clusters, separated by an intermediate zone, are apparent. The bottom panel shows the same correlation matrix reordered to cut two clusters (a dendrogram is shown at the bottom, based on a Spearman metric using the unweighted pair group method with arithmetic mean). The purple cluster of the dendrogram contains a smaller subcluster that indicates nonzero correlation between signals from the most superficial electrodes and those located in between the two cell clusters. This subcluster corresponds to electrodes located in cerebrospinal fluid (above the pia for the superficial electrode and in the ventricle for the intermediate electrodes). The distribution of activity clusters matches that determined from unit identification in (F). (**F**) Distribution of units recorded from electrodes in (E) along probe depth (*y* axis) and width (*x* axis) (same recording and same night). Cortical (Ctx) units, purple; DVR units, red. Each unit's position in space is determined by triangulation across the electrodes and is indicated by a vertical dash. The region between 300 and 400 μm has reduced unit density. Each waveform represents the firing rate around a sharp wave (±1000 ms from the trough of the LFP sharp wave; peak-to-peak amplitudes are normalized). Single-unit firing rate distributions were uniform within each cell population, with cortical units locked and delayed relative to DVR units. Asterisks indicate well-isolated single units (materials and methods). (**G**) Firing rate distributions (in spikes per second) locked to the sharp-wave LFP trough ($t = 0$) for nine DVR single units (SU, stippled red), 230 DVR multi-units (MU, solid red), 21 cortical SUs (stippled purple), and 66 cortical MUs (solid purple) during SWS. (**H**) Firing rate distributions of the units in (G), but around the transition between low and high δ/β (i.e., over all sleep cycles). Firing rates covary and are higher in the cortex at all times (fig. S10).

of cats (*41*) and in the amygdaloid complex of rats, which expresses both slow and fast rhythms (but no ripple-like events during SWS) (*42*). Conversely, rat hippocampal firing patterns during cortical slow waves (*43*) resemble the cortical firing in *Pogona* around DVR sharp waves. Further work is thus needed to clarify the relationship between DVR, a dominant part of the reptilian forebrain, and its potential mammalian equivalent (*44*).

Recent work on mammalian hippocampal ripples focuses on their potential importance for memory transfer and consolidation through accelerated replay of awake-state activity and activation of synaptic plasticity rules in cortical targets (*32*, *33*). In rats, correlations between CA1 ripples and cortical spindles have been demonstrated (*26*). Our results in a reptile suggest that there is also a functional relationship between the DVR and cortex. The projections between the DVR and cortex are extensive, direct, and reciprocal. This offers an opportunity to test the potential generality of the principle whereby sleep ripples participate in memory transfer and consolidation. More generally, the existence of sleep-related dynamics in the brains of reptiles may shed new light on general principles of information processing during sleep.

REFERENCES AND NOTES

1. A. P. Vorster, J. Born, *Neurosci. Biobehav. Rev.* **50**, 103–119 (2015).
2. R. Allada, J. M. Siegel, *Curr. Biol.* **18**, R670–R679 (2008).
3. R. V. Rial *et al*., *Neurosci. Biobehav. Rev.* **34**, 1144–1160 (2010).
4. C. Smith, *Neurosci. Biobehav. Rev.* **9**, 157–168 (1985).
5. J. E. Zimmerman, N. Naidoo, D. M. Raizen, A. I. Pack, *Trends Neurosci.* **31**, 371–376 (2008).
6. D. Bushey, G. Tononi, C. Cirelli, *Science* **332**, 1576–1581 (2011).
7. P. S. Low, S. S. Shank, T. J. Sejnowski, D. Margoliash, *Proc. Natl. Acad. Sci. U.S.A.* **105**, 9081–9086 (2008).
8. R. J. Greenspan, G. Tononi, C. Cirelli, P. J. Shaw, *Trends Neurosci.* **24**, 142–145 (2001).
9. A. L. Loomis, E. N. Harvey, G. A. Hobart III, *J. Exp. Psychol.* **21**, 127–144 (1937).
10. E. Aserinsky, N. Kleitman, *Science* **118**, 273–274 (1953).
11. M. Jouvet, *Prog. Brain Res.* **18**, 20–62 (1965).
12. R. E. Brown, R. Basheer, J. T. McKenna, R. E. Strecker, R. W. McCarley, *Physiol. Rev.* **92**, 1087–1187 (2012).
13. M. Monnier, *Experientia* **36**, 16–19 (1980).
14. N. C. Rattenborg, *Brain Res. Bull.* **69**, 20–29 (2006).
15. N. C. Rattenborg, D. Martinez-Gonzalez, J. A. Lesku, *Neurosci. Biobehav. Rev.* **33**, 253–270 (2009).
16. J. M. Siegel, *Trends Neurosci.* **31**, 208–213 (2008).
17. R. V. Rial *et al*., *Brain Res. Bull.* **72**, 183–186 (2007).
18. P. A. Libourel, A. Herrel, *Biol. Rev. Camb. Philos. Soc.* (2015).
19. J. A. Hobson, *Nature* **437**, 1254–1256 (2005).
20. W. F. Flanigan Jr., *Brain Behav. Evol.* **8**, 401–416 (1973).
21. K. Hartse, in *Principles and Practice of Sleep Medicine*, M.H. Kryger, T. Roth, D.W. Dement, Eds. (Elsevier Saunders, ed. 2, 1994), pp. 95–104.
22. F. Ayala-Guerrero, G. Mexicano, *Comp. Biochem. Physiol. A* **151**, 305–312 (2008).
23. G. F. Striedter, *J. Comp. Neurol.* **524**, 496–517 (2016).
24. The animals, which were raised in controlled feeding, light, and temperature conditions (see the materials and methods section in the supplementary materials), were observed continuously by means of video and physiological monitoring over epochs of 18 to 20 hours in a familiar experimental arena. Light-dark cycles were identical and synchronized to those in their home terrarium. About 1 to 2 hours before normal nighttime (daylight off), the lizards spontaneously became drowsy, settled in one location, and started closing their eyes intermittently (Fig. 1B). During this pre-sleep phase, axial and limb postural tone decreased until the animals assumed a fully relaxed, horizontal sleeping posture with their heads resting on the floor. Their cardiac rhythms decreased over 1 to 2 hours from 40 to 60 beats per minute (bpm) in the awake state to 20 to 30 bpm, by which time their eyes were closed. A low heart rate was maintained throughout the night, except for occasional peaks correlated with brief body repositioning. Toward the end of the night, the lizards' postural tone increased, and they slowly lifted their heads; they opened their eyes, intermittently at first, then reliably at or shortly after the onset of light (Fig. 1B).
25. J. Voigts, J. H. Siegle, D. L. Pritchett, C. I. Moore, *Front. Syst. Neurosci.* **7**, 8 (2013).
26. A. G. Siapas, M. A. Wilson, *Neuron* **21**, 1123–1128 (1998).
27. J. O'Keefe, *Exp. Neurol.* **51**, 78–109 (1976).
28. G. Buzsáki, Z. Horváth, R. Urioste, J. Hetke, K. Wise, *Science* **256**, 1025–1027 (1992).
29. G. Buzsáki, *Hippocampus* **25**, 1073–1188 (2015).
30. A. Draguhn, R. D. Traub, D. Schmitz, J. G. Jefferys, *Nature* **394**, 189–192 (1998).
31. J. M. Siegel, in *Principles and Practice of Sleep Medicine*, M. H. Kryger, T. Roth, W. C. Dement, Eds. (Elsevier Saunders, ed. 4, 2005), pp. 120–135.
32. D. J. Foster, M. A. Wilson, *Nature* **440**, 680–683 (2006).
33. M. A. Wilson, B. L. McNaughton, *Science* **265**, 676–679 (1994).
34. J. Lu, D. Sherman, M. Devor, C. B. Saper, *Nature* **441**, 589–594 (2006).
35. F. Weber *et al*., *Nature* **526**, 435–438 (2015).
36. J. A. Hobson, R. W. McCarley, P. W. Wyzinski, *Science* **189**, 55–58 (1975).
37. Y. Hayashi *et al*., *Science* **350**, 957–961 (2015).
38. C. B. Saper, T. C. Chou, T. E. Scammell, *Trends Neurosci.* **24**, 726–731 (2001).
39. C. B. Saper, T. E. Scammell, J. Lu, *Nature* **437**, 1257–1263 (2005).
40. R. G. Northcutt, *Annu. Rev. Neurosci.* **4**, 301–350 (1981).
41. F. Grenier, I. Timofeev, M. Steriade, *J. Neurophysiol.* **86**, 1884–1898 (2001).
42. D. Paré, D. R. Collins, J. G. Pelletier, *Trends Cogn. Sci.* **6**, 306–314 (2002).
43. A. Sirota, J. Csicsvari, D. Buhl, G. Buzsáki, *Proc. Natl. Acad. Sci. U.S.A.* **100**, 2065–2069 (2003).
44. H. J. Karten, *Brain Behav. Evol.* **38**, 264–272 (1991).

ACKNOWLEDGMENTS

This research was funded by the Max Planck Society and the European Research Council (G.L.) and by fellowships from the Minerva Foundation (M.S.-I.) and the Swiss National Science Foundation (J.M.O.). The code for analysis and partial data are available at www.brain.mpg.de/sheinidelsonetal2016, and the full primary data are available from G.L. on request. The authors are grateful to G. Wexel for help in surgery and postoperative care; M. Klinkmann, A. Arends, Á. M. Pardo, T. Manthey, and C. Thum for technical assistance; F. Baier, T. Maurer, G. Schmalbach, and A. Umminger for help with mechanical design and fabrication; N. Heller for help with electronics; K. Schröder and C. Schürmann (Goethe University Medical School, Institute for Cardiovascular Physiology) for help with μ-CT scanning of lizards; the animal caretaker crew for lizard care; and T. Tchumatchenko, H. Ito, M. Kaschube, E. Schuman, A. Siapas, and the Laurent laboratory for their suggestions during the course of this work or on the manuscript.

SUPPLEMENTARY MATERIALS

www.sciencemag.org/content/352/6285/590/suppl/DC1
Materials and Methods
Figs. S1 to S10
References (*45*–*53*)
Movie S1

29 January 2016; accepted 1 April 2016
10.1126/science.aaf3621

SIGNAL TRANSDUCTION

Phase separation of signaling molecules promotes T cell receptor signal transduction

Xiaolei Su,[1,2]* Jonathon A. Ditlev,[1,3]* Enfu Hui,[1,2] Wenmin Xing,[1,3] Sudeep Banjade,[1,3] Julia Okrut,[1,2] David S. King,[4] Jack Taunton,[1,2] Michael K. Rosen,[1,3]† Ronald D. Vale[1,2]†

Activation of various cell surface receptors triggers the reorganization of downstream signaling molecules into micrometer- or submicrometer-sized clusters. However, the functional consequences of such clustering have been unclear. We biochemically reconstituted a 12-component signaling pathway on model membranes, beginning with T cell receptor (TCR) activation and ending with actin assembly. When TCR phosphorylation was triggered, downstream signaling proteins spontaneously separated into liquid-like clusters that promoted signaling outputs both in vitro and in human Jurkat T cells. Reconstituted clusters were enriched in kinases but excluded phosphatases and enhanced actin filament assembly by recruiting and organizing actin regulators. These results demonstrate that protein phase separation can create a distinct physical and biochemical compartment that facilitates signaling.

Many cell surface receptors and downstream signaling molecules coalesce into micrometer- or submicrometer-sized clusters upon initiation of signaling (*1*, *2*). However, the effect of this clustering on signal transduction is poorly understood. T cell receptor (TCR) signaling is a well-studied example of this general phenomenon (*3*). TCR signaling proceeds through a series of biochemical reactions that can be viewed as connected modules. In the upstream module, the TCR is phosphorylated by Lck, a membrane-bound protein kinase of the Src family. TCR phosphorylation is opposed by a transmembrane phosphatase, CD45 (*3*). The phosphorylated cytoplasmic domains of the TCR complex recruit and activate the cytosolic tyrosine kinase ZAP70 (*4*). In the intermediate module, ZAP70 phosphorylates the transmembrane protein LAT (linker for activation of T cells) on multiple tyrosine residues. These phosphotyrosines

Slow waves, sharp waves, ripples, and REM in sleeping dragons

Mark Shein-Idelson, Janie M. Ondracek, Hua-Peng Liaw, Sam Reiter and Gilles Laurent

Science **352** (6285), 590-595.
DOI: 10.1126/science.aaf3621

The dragon sleeps tonight

Most animal species sleep, from invertebrates to primates. However, neuroscientists have until now only actively recorded the sleeping brains of birds and mammals. Shein-Idelson *et al.* now describe the electrophysiological hallmarks of sleep in reptiles. Recordings from the brains of Australian dragons revealed the typical features of slow-wave sleep and rapid eye movement (REM) sleep. These findings indicate that the brainstem circuits responsible for slow-wave and REM sleep are not only very ancient but were already involved in sleep dynamics in reptiles.

Science, this issue p. 590